CIVL 598L Project

Daniel Robb

Preliminaries

This paper is divided into Part 1 and Part 2. In Part 1, I examine the propagation of weakly nonlinear internal waves in a closed basin; in Part 2, I examine surface gravity waves in counter-propagating flows over an obstacle.

Part 1: Internal waves in a two-layer system

1 Introduction

Internal waves play an important role in the transport of heat, nutrients, and other scalars in lakes and reservoirs. Internal wave breaking leads to enhanced mixing between layers in a density stratified fluid. Predicting the mixing processes in a lake requires an understanding of the mechanisms controlling the generation, evolution, and degeneration of internal waves. Here, I focus on interfacial gravity waves in a two-layer system.

When the wind blows over a lake, a stress is applied to the water surface, which tilts the water surface in the downwind direction. To maintain a hydrostatic pressure gradient, the thermocline tilts in the opposite direction. Since the density difference between the two layers is typically small, the deflection of the thermocline is much larger than that of the water surface.

After the wind stops, there is no longer an applied stress at the water surface to maintain the surface and interfacial tilts, and as a result, basin-scale seiches develop — one on the water surface and one on the interface. The amplitude of the water surface seiche is typically small and will no longer be considered here. The amplitude of the interfacial seiche, however, can be large, reaching the height of the epilimnion.

Interfacial waves resulting from wind setup are often described using linear wave theory (Mortimer 1952); however, field observations have shown that wave amplitudes can be large enough so that nonlinear effects become important (Farmer 1978). These nonlinear effects can have important consequences on the physical processes in the water body. For example, nonlinear steepening can transfer wave energy from the basin scale to shorter length scales, generating packets of shorter waves. These shorter waves, or *solitons*, are prone to shoal at sloping boundaries, resulting in enhanced boundary mixing (Horn et al. 2002).

The goal in Part 1 is to describe the weakly nonlinear model from Horn et al. (2002) that was used to predict the evolution of interfacial waves in a closed basin. As a component of this project, I wrote a computer code to try to reproduce the results presented in Horn et al. (2002). The rest of Part 1 is organized as follows. In section 2, I present the theoretical formulation used here to study weakly nonlinear interfacial waves resulting from wind setup. In section 3, I describe the numerical method

used to compute the results presented herein. Finally, in section 4, I show a set of numerical results starting with the simplest and gradually becoming more complex.

2 Theoretical formulation

The equations of motion used to compute the results in Part 1 are for long weakly nonlinear and weakly dispersive waves. I will first address the nonlinearity and then the dispersive nature of these waves.

2.1 Long weakly nonlinear waves

Starting with the Saint-Venant equations in one dimension, conservation of mass and momentum are:

$$\frac{\partial h}{\partial t} + \frac{\partial (hu)}{\partial x} = 0, \tag{1}$$

$$\frac{\partial u}{\partial t} + u\frac{\partial u}{\partial x} + g\frac{\partial h}{\partial x} = 0, \tag{2}$$

where $h(x,t)$ is the depth of water from the free surface to the bottom, $u(x,t)$ is velocity, g is gravitational acceleration and x and t are coordinates of space and time, respectively. The depth of water $h = H + \eta(x,t)$, where H is a constant depth. These equations describe nonlinear shallow flows with long (non-dispersive) waves.

Equations (1) and (2) can be written in vector form:

$$\frac{\partial}{\partial t}\begin{pmatrix} u \\ h \end{pmatrix} + \begin{pmatrix} u & g \\ h & u \end{pmatrix}\frac{\partial}{\partial x}\begin{pmatrix} u \\ h \end{pmatrix} = 0. \tag{3}$$

We can transform the coordinate system to be moving with a right-moving characteristic curve $X_+ = x - c_+ t$. Calculating the eigenvalues of the matrix in (3), gives $c_\pm = u \pm \sqrt{gh}$, and taking the right-moving one, it can be shown the $u_{X_+} = \sqrt{(g/h)}h_{X_+}$ and that $r_\pm \equiv u \pm 2\sqrt{gh}$ is constant along the right (left)-moving characteristic curves. Following Sutherland (2010) Chp. 4, we use r_- as an initial condition for the rightward-propagating wave; therefore:

$$u = 2\sqrt{gh} - 2\sqrt{gH} \tag{4}$$

along characteristic curves X_+. Substituting (4) into (eq:mass) and noting that $h = H + \eta$:

$$\frac{\partial \eta}{\partial t} + \left(3\sqrt{g(H+\eta)} - 2\sqrt{gH}\right)\frac{\partial \eta}{\partial x} = 0. \tag{5}$$

If $\eta/H \ll 1$, then the linear wave equation is recovered, where $c_0 = \sqrt{gH}$. If we consider η to be non-negligible, then we can see that waves with $\eta > 0$ will move faster than those with $\eta < 0$. This means the wave will steepen as the crests catch up to the troughs and the wave may begin to break.

Let's consider η/H to be a small parameter ϵ, then

$$\sqrt{g(H+\eta)} = c_0\sqrt{1+\epsilon} \approx c_0\left(1+\frac{1}{2}\epsilon+...\right), \tag{6}$$

and neglecting terms of $\mathcal{O}(\epsilon^2)$ or higher, (5) becomes

$$\eta_t + c_0\eta_x + \frac{3}{2}\frac{c_0}{H}\eta\eta_x = 0. \tag{7}$$

The nonlinear term in (7) appears in the model equations that are solved in the present study. They account for weakly nonlinear effects of long waves.

2.2 Weakly dispersive waves

Under a different set of assumptions as above, let's consider linear dispersive waves with the dispersion relation

$$\omega = \sqrt{gk\tanh kH}, \tag{8}$$

where ω is the frequency and k is the wave number. For small values of kH, $\tanh(kH) \approx kH$ and (8) reduces to $\omega/k = \sqrt{gH} = c_0$, i.e., the shallow water wave speed, which does not depend on k, so these are non-dispersive waves. If we let kH be a small parameter ϵ then:

$$\omega = \sqrt{gk\tanh kH} \approx \sqrt{gk}\left(\epsilon^{1/2} - \frac{1}{6}\epsilon^{5/2} + ...\right) = \sqrt{gk}\left(\sqrt{kH} - \frac{(kH)^{5/2}}{6}\right) = c_0k - \frac{c_0H^2}{6}k^3. \tag{9}$$

For linear waves, we look for solutions in the form:

$$\eta(x,t) = A\exp\left[i(kx-\omega t)\right]. \tag{10}$$

From Whitham (1974) Chp. 11, a linear equation with constant coefficients can be written as:

$$P\left(\frac{\partial}{\partial t}, \frac{\partial}{\partial x}\right)\eta = 0, \tag{11}$$

where P is a polynomial. Substituting the lefthand side of (10) into (11) gives:

$$P(-i\omega, ik) = 0, \tag{12}$$

which is the dispersion relation for (10). Therefore, given the dispersion relation in (9), the corresponding linear equation is:

$$\eta_t + c_0\eta_x + \frac{1}{6}c_0H^2\eta_{xxx} = 0. \tag{13}$$

2.3 The Korteweg-de Vries equation

For a weakly nonlinear, weakly dispersive wave where the nonlinear and dispersion terms or of the same order, we can use (7) and (13) to give

$$\eta_t + c_0\eta_x + \frac{3}{2}\frac{c_0}{H}\eta\eta_x + \frac{1}{6}c_0H^2\eta_{xxx} = 0. \tag{14}$$

Equation 14 is the Korteweg-de Vries (KdV) equation, which I solve numerically in section 4. If we neglect the third and fourth terms on the righthand side of (14), the linear non-dispersive wave equation is recovered. If the third and fourth terms are of the same order, then $a/H \sim (H/L)^2$, where a is a measure of wave amplitude, H is the vertical scale and L is a measure of the wave length.

There are many variants of the KdV equation; here we focus on a variant in the form:

$$\eta_t + (c_0 + \alpha\eta)\eta_x + \beta\eta_{xxx} = 0. \tag{15}$$

For a surface gravity wave, $c_0 = \sqrt{gH}$, $\alpha = \frac{3}{2}\frac{c_0}{H}$, and $\beta = \frac{1}{6}c_0H^2$ and H is the water depth.

2.4 The Korteweg-de Vries equation for an interfacial gravity wave

For an interfacial gravity wave in a two-layer system where the density differences between layers are small, the KdV equation can have the same form as in (15) but the coefficients will differ. If we define a reduced gravity as:

$$g' = g\frac{\rho_2 - \rho_1}{\bar{\rho}}, \tag{16}$$

then

$$c_0 = \sqrt{g'\frac{h_1h_2}{h_1 + h_2}}, \quad \alpha = \frac{3}{2}c_0\frac{h_1 - h_2}{h_1h_2}, \quad \text{and} \quad \beta = \frac{1}{6}c_0h_1h_2, \tag{17}$$

as described in Helfrich and Melville (2006). In (16) and (17), the subscripts 1 and 2 stand for the top and bottom layer, respectively.

In the next section, I will describe the numerical method used to solve (15).

3 Numerical method

The numerical method in the present study follows Fornberg and Whitham (1978) and is summarized herein. Consider the KdV equation

$$u_t + uu_x + u_{xxx} = 0. \tag{18}$$

The variable $u(x,t)$ is transformed into Fourier space with respect to x so that derivatives with respect to x become algebraic, which reduces the partial differential equation to an ordinary differential

equation with respect to t. The transformation between real space and wave number space, and vice versa, are performed using the Fourier transform:

$$\hat{u}(k) = \mathcal{F}\left[u(x)\right] = \int_{-\infty}^{\infty} u(x)\exp(-ikx)dx \approx \sum_{m=0}^{n-1} u(x)\exp\left(-i\frac{mk}{n}\right), \tag{19}$$

and the inverse Fourier transform:

$$u(x) = \mathcal{F}^{-1}\left[\hat{u}(k)\right] = \int_{-\infty}^{\infty} \hat{u}(k)\exp(ikx)dk \approx \frac{1}{n}\sum_{m=0}^{n-1} \hat{u}(k)\exp\left(i\frac{mk}{n}\right), \tag{20}$$

written here in both continuous and discrete forms. Equation 18 can then be solved numerically by representing the temporal derivatives as finite differences, and with a leap-frog time stepping scheme, the discrete solution is given by:

$$\frac{u(x,t+\Delta t) - u(x,t-\Delta t)}{2\Delta t} + u\mathcal{F}^{-1}\left[ik\mathcal{F}(u)\right] + \mathcal{F}^{-1}\left[-ik^3\mathcal{F}(u)\right] = 0, \tag{21}$$

where the $u = u(x,t)$ in the second and third terms. This numerical method above was used to compute the results presented in the next section.

4 Results

Two sets of numerical results are presented. First, using the code developed in the present study, numerical results are compared to the classical numerical experiments from Zabusky and Kruskal (1965). Then, after adapting the code to simulate interfacial waves, I reproduce numerical and laboratory experiments from Horn et al. (2002).

4.1 Solitons

To verify that the numerical model developed in the present study reproduces the expected results, I compare them to those presented in Zabusky and Kruskal (1965). They solve the KdV equation of the form:

$$u_t + uu_x + \delta^2 u_{xxx} = 0, \tag{22}$$

with initial conditions $u(x,0) = \cos(\pi x)$, periodic boundary conditions on the interval $0 \leq x < 2$, and $\delta^2 = 0.022$. Note, (22) is equivalent to (15) for $c_0 = 0$, $\alpha = 1$, and $\beta = 0.022$.

A side-by-side comparison of the computed results from Zabusky and Kruskal (1965) with those computed in the present study show good agreement (Fig. 1). The good agreement provides some confidence that the numerical model in the present study working as intended. More rigorous validation would include comparing the computed results to an analytical solution and calculating the error (e.g. L2-norm error) for increasingly fine spatial resolutions to determine (a) if the computed results converge to the known solution and (b) at what spatial resolution do the results become mesh independent.

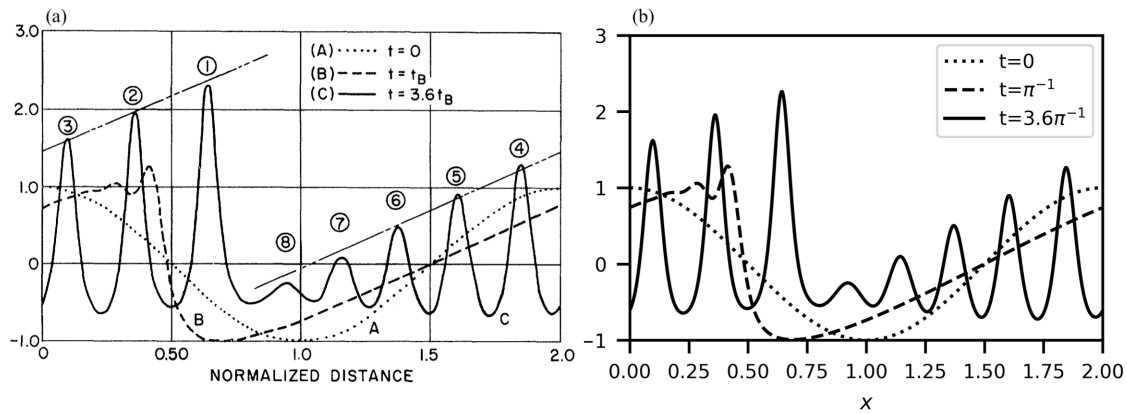

Figure 1: Temporal development of the wave $u(x,t)$ a $t = 0,\ \pi^{-1},$; and $3.6\pi^{-1}$. (a) Numerical results from Zabusky and Kruskal (1965); (b) Numerical results from the present study.

4.2 Weakly nonlinear long internal waves in closed basins

The numerical method applied in the previous section is now adapted for interfacial wave propagation in a closed basin. The equations of motion are nearly the same as in (15) with constant coefficients determined by (17). A dissipative term is added to (15) to account for laminar boundary layers along solid surfaces (see Horn et al. (2002) section 2.2 for details).

The objective here is to simulate weakly nonlinear interfacial waves in a closed basin and to compare the predictions in the present study to laboratory and numerical results in Horn et al. (2002). The motivation is to understand two-layer wave propagation arising from an initial tilt of the interface — an idealization of interfacial waves generated by wind setup in lakes.

To study weakly nonlinear internal wave propagation in a closed basin, Horn et al. (2002) conducted laboratory experiments in a long tank that could rotate about a horizontal axis so that the interface of a two-layer fluid could be initially tilted (Fig. 2). The experiment started at $t = 0$ when the tank was suddenly returned to a horizontal position. The interfacial tilt resulted in internal wave propagation which was recorded by wave gauges at several locations (Fig. 2).

In Horn et al. (2002), a numerical model was developed to study the internal wave propagation under a variety of conditions. They use a Fourier (pseudospectral) method like the one presented in section 3. Since the KdV equation is uni-directional and this physical problem has waves propagating to the right and to the left, the authors applied a method of reflection where they extend the physical bi-directional domain to form a uni-directional domain of twice the former's length. Given the initial conditions and the method of reflection described in Horn et al. (2002), the authors were able to simulate bi-directional wave propagation from solutions to the KdV equation. The same method was used to compute the results in the present study.

Comparisons of results from Horn et al. (2002) to results from the present study show good agreement (Fig. 3; Fig. 4). The results demonstrate the utility of the numerical model in the present study to simulate weakly nonlinear internal waves in a two-layer system.

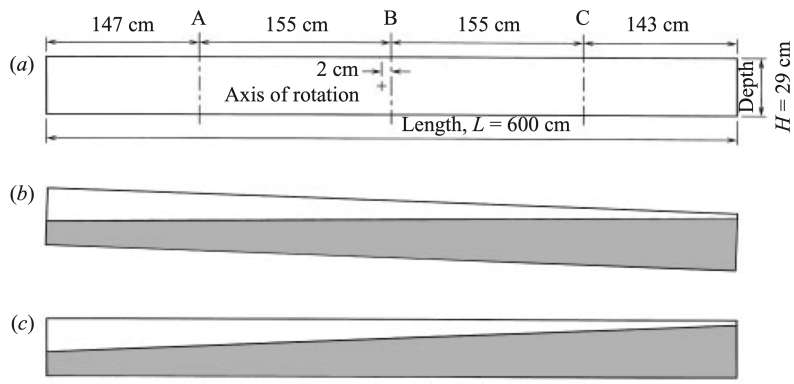

Figure 2: From Horn et al. (2002). (a) Schematic diagram of the experimental set-up. The ultrasonic wavegauges were located at the positions marked A, B and C. (b, c) The tank and the density structure immediately before and after an experiment commences: (b) initially tilted tank, (c) initial condition with the tank horizontal and interface inclined.

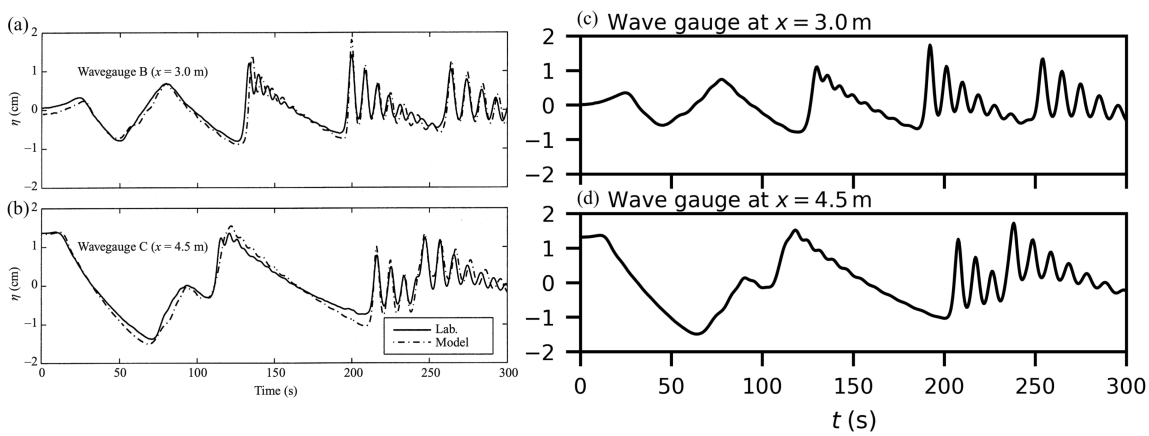

Figure 3: Comparison of observed and simulated interface displacements. Time series of interfacial displacements at wave gauges B ($x = 3.0\,\mathrm{m}$) and C ($x = 4.5\,\mathrm{m}$). (a, b) from Horn et al. (2002); (c, d) present study; (a, c) wave gauge B; (b, d) wave gauge C. For this experiment $h_1 = 23.2\,\mathrm{cm}$, $h_2 = 5.8\,\mathrm{cm}$, $\theta = 0.5°$, and $\Delta\rho = 20\,\mathrm{kg\,m^{-3}}$.

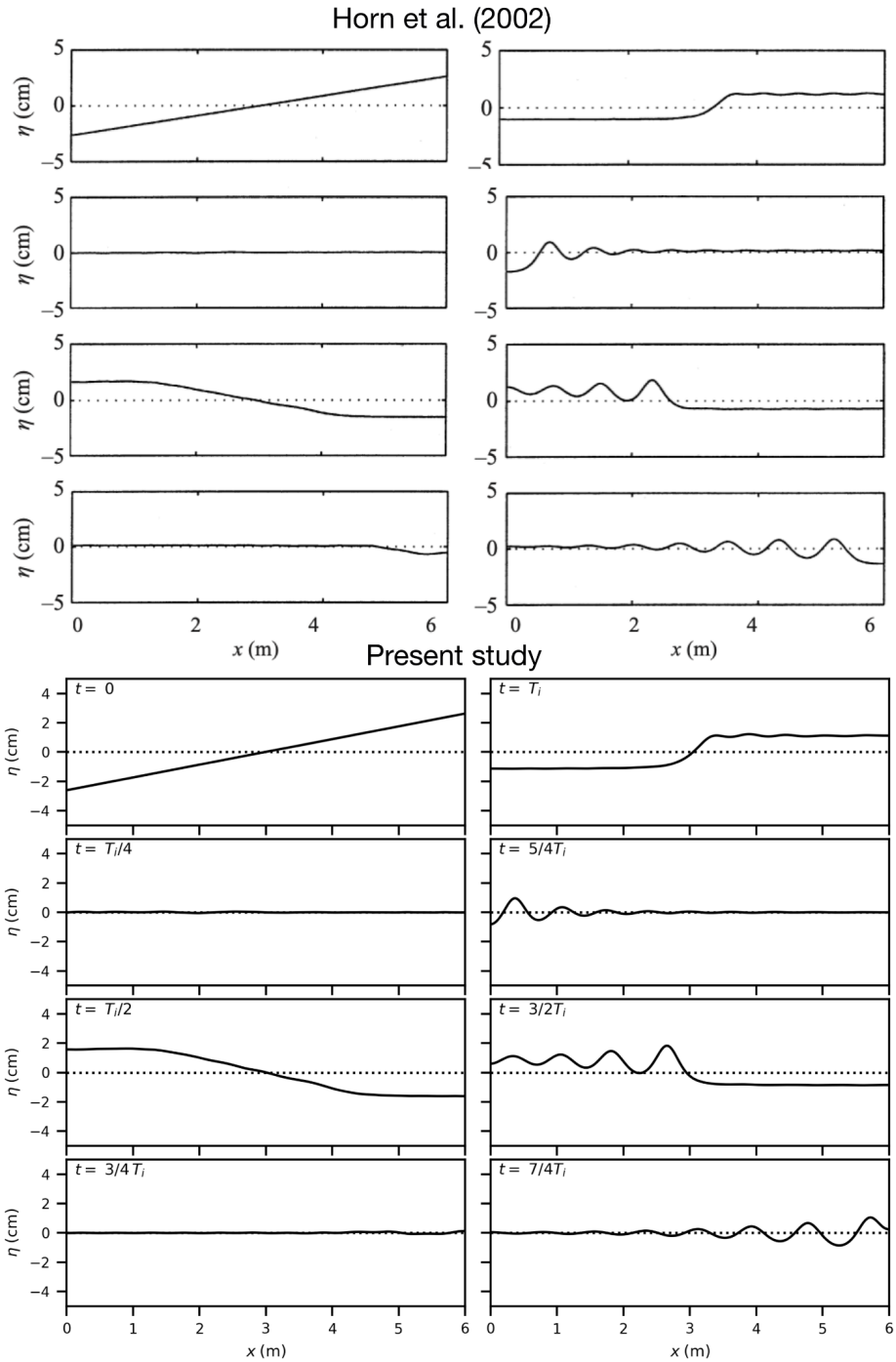

Figure 4: Comparison of simulated interface displacements plotted at intervals of $T_i/4$ where T_i is the basin seiche period. (top) results from Horn et al. (2002); (bottom) results from the present study. For this experiment $h_1 = 23.2\,\mathrm{cm}$, $h_2 = 5.8\,\mathrm{cm}$, $\theta = 0.5°$, and $\Delta\rho = 20\,\mathrm{kg\,m^{-3}}$.

Part 2: Surface gravity waves in a steady flow over an obstacle

5 Introduction

The motivation of Part 2 was to apply the theory presented in *Low-frequency analogue Hawking radiation: The Korteweg–de Vries model* by Coutant and Weinfurtner (2018) to the laboratory experiments described in Weinfurtner et al. (2011) and Lawrence et al. (2012). While some initial effort was put into linking the theory presented in these studies, given the time constraints for the CIVL 598L project this idea was abandoned. Instead, I will present a mathematical formulation and numerical method for studying wave-current interaction problems like those described in Weinfurtner et al. (2011) and Lawrence et al. (2012). The rest of Part 2 is organized as follows. In section 6, I present the theoretical formulation used here to study linear surface gravity waves in an inhomogeneous flow. In section 7, I describe the numerical method used to compute the results presented herein. In section 8, I show numerical results similar to those presented in Unruh (1995). Finally, in section 9, I propose some future directions.

6 Theoretical formulation

Consider an incompressible, inviscid, irrotational fluid in two dimensions in the xz-plane (Fig. 5). There is a no penetration condition along the bottom boundary and a free-surface condition on the top boundary. A steady current flows to the left and a counter-propagating linear surface gravity wave travels to the right. An obstacle gives rise to a water depth $h(x)$ and velocity $v(x)$ that vary over the obstacle. Since the wave properties,(e.g. frequency ω, wave number k, phase speed c_p , group speed c_g) depend on h and v, they too vary over the obstacle.

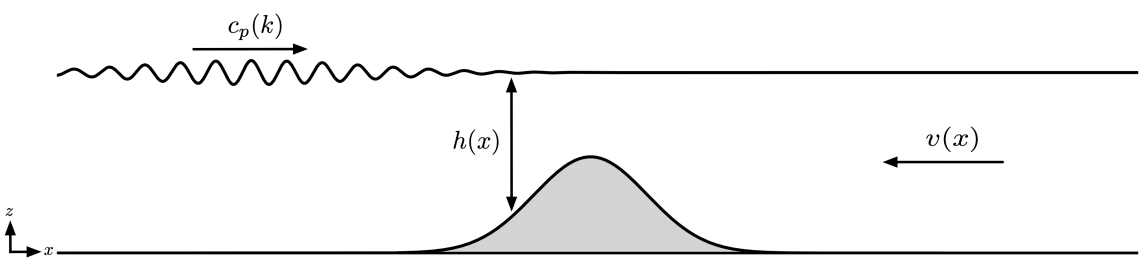

Figure 5: Problem definition sketch. A surface gravity wave propagates to the right with a phase speed $c_p(k)$ in a counter-propagating current with velocity $v(x)$. The presence of the obstacle gives rise to an inhomogeneous flow.

In a stationary wave field, the dispersion relation for a linear surface gravity wave is:

$$\omega^2 = gk \tanh kh \tag{23}$$

but in the presence of a current, the wave is doppler shifted, so (23) becomes

$$\Omega^2 = (\omega - vk)^2 = gk \tanh kh, \tag{24}$$

where $\Omega(k)$ is the frequency as seen from an observer travelling with the mean flow (i.e., the intrinsic frequency in the co-moving frame) and $\omega(k)$ is the frequency as seen by a stationary observer (i.e., the local frequency in the laboratory frame).

The generated waves have wave lengths that are long compared to the depth of water, so they are shallow water waves and they are non-dispersive, but as they approach the obstacle, $v(x)$ becomes more negative. Since ω remains constant, k must increase, resulting in shorter wavelengths. With shorter wavelengths compared to the water depth, dispersive effects become important and the waves are no longer shallow water waves. An approach that can account for these effects is presented in Lawrence et al. (2012) and Robertson, Michel, and Parentani (2016).

Starting with equation (15) from Lawrence et al. (2012), the perturbation velocity potential ϕ caused by the waves on a background flow is

$$\frac{\partial^2\phi}{\partial t^2} + \frac{\partial}{\partial t}\left(v(x)\frac{\partial\phi}{\partial x}\right) + \frac{\partial}{\partial x}\left((v(x)^2 - c(k)^2)\frac{\partial\phi}{\partial x}\right) + \frac{\partial}{\partial x}\left(v(x)\frac{\partial\phi}{\partial t}\right) = 0, \tag{25}$$

which can be re-written to give

$$(\partial_t + \partial_x v(x))(\partial_t + v(x)\partial_x)\phi + f^2(i\partial_x)\phi = 0, \tag{26}$$

where

$$f^2(k) = gk\tanh(kh) \approx gk(kh - \frac{1}{3}(kh)^3) = c_0^2k^2(1 - \frac{1}{3}(kh)^2), \tag{27}$$

and

$$f^2(i\partial_x)\phi(x,t) = \mathcal{F}^{-1}\left[f^2(k)\hat{\phi}(k,t)\right]$$

and substituting the approximation on the righthand side of (27) into (26) gives

$$(\partial_t + \partial_x v(x))(\partial_t + v(x)\partial_x)\phi - c_0^2\partial_x^2\phi - \frac{1}{3}c_0^2h^2\partial_x^4\phi = 0. \tag{28}$$

In the next section, I will describe the numerical method used to solve (26).

7 Numerical method

The numerical method used to compute the results presented herein followed Unruh (1995) and Robertson (2011). To include dispersive effects resulting in the higher order spatial derivatives, they use a similar Fourier method as described in Part 1 of this paper.

8 Results

I simulated a wave packet propagating against a current for a variety of background flow conditions. Simulation results are shown for six different background flows (Fig. 6). The location of the obstacle is indicated by the vertical dashed lines. The colour gradient shows the variation in perturbation velocity potential. Outside the vertical dashed lines, the background flow has a Froude number equal to Fr_{min} and inside the dashed lines, the Froude number increases smoothly to Fr_{max} at $x = 0.75$.

The background velocity profile was

$$v(x) = \frac{1}{2}(Fr_{max} - Fr_{min}) \tanh\left[24\cos\left(2\pi(x - 0.25)\right) + 23\right] - \frac{1}{2}(Fr_{max} + Fr_{min}), \tag{29}$$

which is the same shape as in Unruh (1995). The initial wave velocity potential was

$$\phi(x, 0) = \frac{\sigma}{2} \exp\left(-\frac{(x - x_0)^2}{2\sigma^2} + 8i\frac{x - x_0}{\sigma}\right), \tag{30}$$

where $\sigma = 0.05$, $x_0 = 0.3$, and $i = \sqrt{-1}$. Simulations were run with a spatial discretization of $\Delta x = 1/2048$ on a domain $x \in [0, 1)$ with periodic boundary conditions.

From Fig. 6, the wave passes over the obstacle for $Fr_{max} \leq 0.5$ and the wave is blocked for $Fr_{max} \geq 0.7$, where $Fr_{min} = Fr_{max} - 0.4$ in all cases. For $Fr_{max} = 0.6$, the incident wave is partially arrested such that shorter waves are reflected downstream to the left and longer waves are transmitted to the right over the obstacle.

Videos showing the variation in velocity potential with space and time are provided as supplementary material. They can be viewed at https://youtu.be/xKXcPcEFGmQ .

9 Future directions

The results presented herein could be extended in a number of ways. A few future directions are listed below:

- Simulate numerically the Vancouver experiment presented in Weinfurtner et al. (2011) and Lawrence et al. (2012)
- Review Robertson, Michel, and Parentani (2016) who discuss scattering of subcritical waves of obstacles of different shapes and they discuss the Vancouver experiment presented in Weinfurtner et al. (2011) and Lawrence et al. (2012)
- Review the paper *Minimal analytical model for undular tidal bore profile; quantum and Hawking effect analogies* by Berry (2018) who compares his analytical model to undular bore data from Chanson
- Predict the properties of the outgoing waves (e.g. amplitude, phase speed) for various background flows and incoming waves.
- Link the theory Lawrence (1987) to the theory in Lawrence et al. (2012)?
- Connect the theory presented in Coutant and Weinfurtner (2018) on the KdV model to previous work in Weinfurtner et al. (2011)

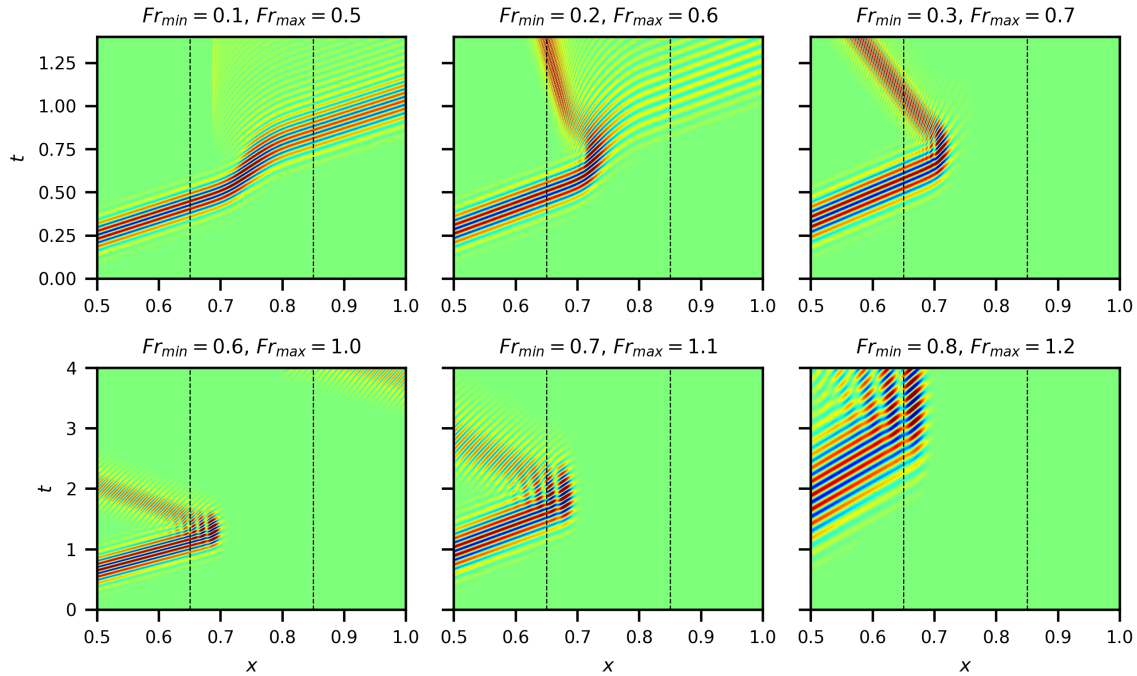

Figure 6: Velocity potential plotted as a function of space and time for a packet of waves propagating against a current with Froude numbers Fr as indicated on the respective panels. Fr_{min} occurs far away from the obstacle and Fr_{max} occurs at $x = 0.75$, at the crest of the obstacle. $Fr = Fr_{min}$ for $x < 0.65$ and $x > 0.85$ and $Fr_{min} \leq Fr \leq Fr_{max}$ for $0.65 \leq x \leq 0.85$. The vertical dashed lines indicate the extent of the obstacle.

Supplementary material

Videos showing the variation in velocity potential for various background flows are provided here: https://youtu.be/xKXcPcEFGmQ .

References

Berry, MV. 2018. "Minimal analytical model for undular tidal bore profile; quantum and Hawking effect analogies." *New Journal of Physics.*

Coutant, A, and S Weinfurtner. 2018. "Low-Frequency Analogue Hawking Radiation: The Korteweg–de Vries Model." *Physical Review D* 97 (2). APS: 025005.

Farmer, DM. 1978. "Observations of long nonlinear internal waves in a lake." *Journal of Physical Oceanography.*

Fornberg, B, and GB Whitham. 1978. "A numerical and theoretical study of certain nonlinear wave phenomena." *Of the Royal Society of.*

Helfrich, KR, and WK Melville. 2006. "Long nonlinear internal waves." *Annu. Rev. Fluid Mech.*

Horn, DA, J Imberger, GN Ivey, and LG Redekopp. 2002. "A weakly nonlinear model of long internal waves in closed basins." *Journal of Fluid Mechanics* 467: 269–87.

Lawrence, GA. 1987. "Steady Flow over an Obstacle." *Journal of Hydraulic Engineering* 113 (8). American Society of Civil Engineers: 981–91.

Lawrence, GA, S Weinfurtner, EW Tedford, MCJ Penrice, and WG Unruh. 2012. "Waves and Currents: Hawking radiation in the hydraulics laboratory?" *Environmental Fluid Mecahanics: Memorial Volume in Honour of Prof. Gerhard H. Jirka (Ed. W. Rodi & M. Uhlmann).*

Mortimer, CH. 1952. "Water Movements in Lakes During Summer Stratification; Evidence from the Distribution of Temperature in Windermere." *Philosophical Transactions of the Royal Society of London. Series B, Biological Sciences* 236 (635). The Royal Society London: 355–98.

Robertson, SJ. 2011. "Hawking radiation in dispersive media." *arXiv Preprint arXiv:1106.1805.*

Robertson, SJ, F Michel, and R Parentani. 2016. "Scattering of gravity waves in subcritical flows over an obstacle."

Sutherland, BR. 2010. *Internal Gravity Waves.* Cambridge university press.

Unruh, WG. 1995. "Sonic analogue of black holes and the effects of high frequencies on black hole evaporation." *Physical Review D* 51: 2827–38. doi:10.1103/physrevd.51.2827.

Weinfurtner, S, EW Tedford, MCJ Penrice, WG Unruh, and GA Lawrence. 2011. "Measurement of Stimulated Hawking Emission in an Analogue System." *Physical Review Letters* 106: 021302.

Whitham, GB. 1974. *Linear and nonlinear waves.* Modern Book Incorporated.

Zabusky, NJ, and MD Kruskal. 1965. "Interaction of' Solitons' in a Collisionless Plasma and the Recurrence of Initial States." *Physical Review Letters* 15 (6). APS: 240.